Supplementary Figures

Supplementary Figure 1, related to Figure 1

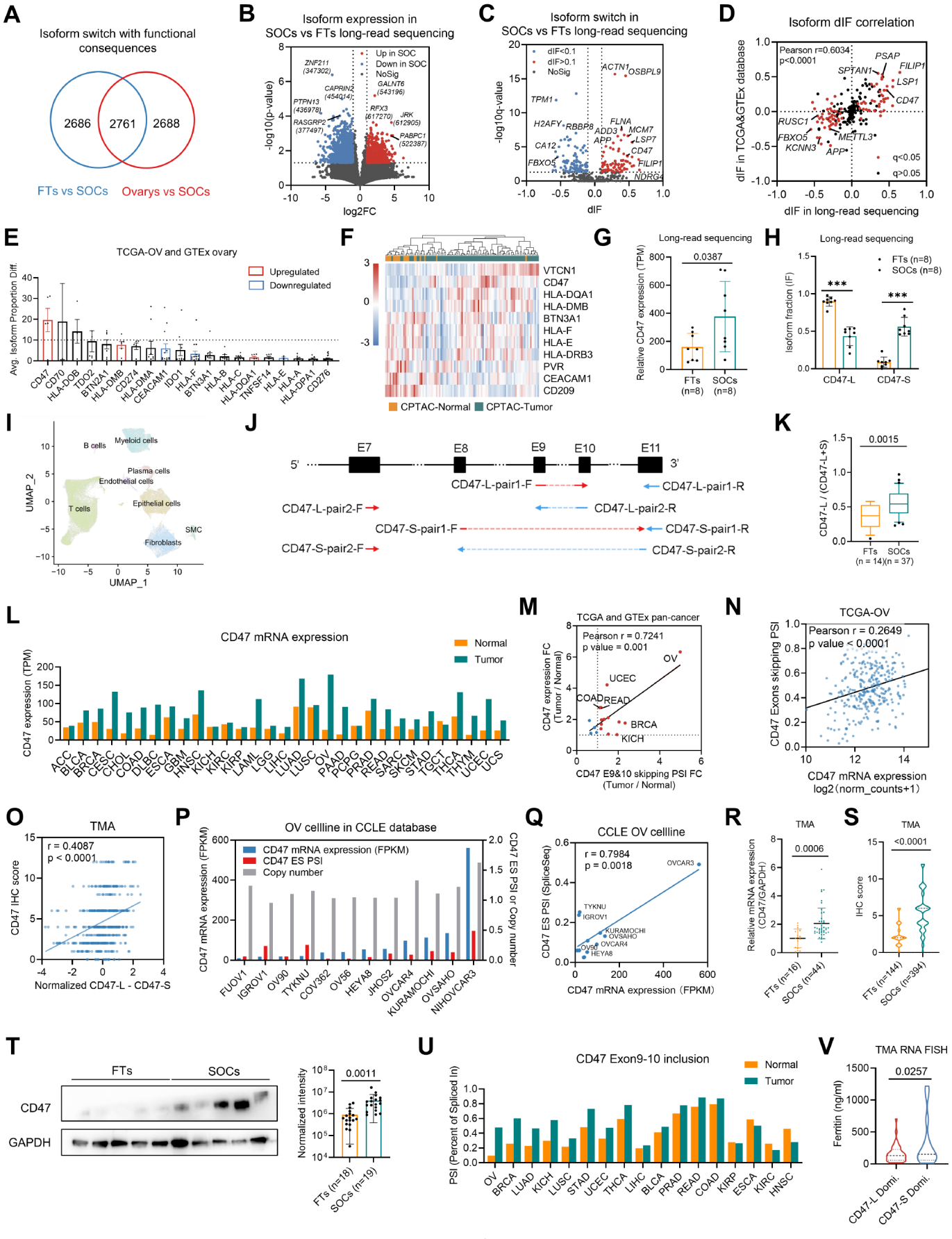

Supplementary Figure 1. Pan-cancer analysis of immune checkpoint CD47 and its isoforms. (A) The Venn diagram demonstrates the common targets analyzed in ovarian cancer with consequence of isoform switching, using normal fallopian tube umbrella tissue or ovarian tissue as control. **(B)** Volcano plot of differential expressed isoforms in long-read RNA sequencing data of 8 pairs of SOCs and FTs. **(C)** Volcano plot of differential Isoform fraction (dIF) of the Isoform switch events. **(D)** Correlation analysis of the isoform switch events in TCGA-OV and GTEx database and our long-read RNA sequencing data. **(E)** Average value of differential isoforms proportion of each immune checkpoint. Data was shown as mean with SEM. **(F)** Heatmap of protein expression pattern of immune checkpoints with significant differential changes in SOCs and normal tissues from CPTAC-PNNL database. **(G, H)** CD47 mRNA expression **(G)** and isoform fraction **(H)** of FTs (n = 8) and SOCs (n = 8) in long-read RNA sequencing data. **(I)** UMAP projection of all cells from scRNA-seq data of FTs (n = 5) and SOCs (n = 5), colored by cell types. **(J)** Schematic diagram of the isoform-specific qPCR primer design scheme for detecting CD47-L and CD47-S. Pair1 primers detected endogenous isoform expression, while Pair2 primers detected exogenous isoform expression. **(K)** qPCR verification of CD47-L ratio in FTs (n = 14) and SOCs (n = 37). **(L)** Pan-cancer analysis of CD47 mRNA expression in TCGA-OV comparing with normal tissue in GTEx database. **(M)** Correlation analysis of differential fold change in CD47 mRNA expression and PSI compared to normal samples across cancer types. **(N)** The correlation analysis of CD47 exon 9 and 10 skipping PSI and mRNA expression in ovarian cancer samples in TCGA-OV. **(O)** Correlation between IHC score of CD47 protein and difference between CD47-L and CD47-S immunofluorescence intensity. **(P)** CD47 mRNA expression, CD47 multi-exon skipping PSI index, and CD47 copy number in CCLE ovarian cancer cell lines. mRNA expression was normalized with FPKM. **(Q)** The correlation analysis of CD47 exon 9 and 10 skipping PSI and mRNA expression in ovarian cancer cell lines in CCLE database. **(R and S)** Relative CD47 mRNA expression **(R)** and IHC score **(S)** of FTs and SOCs in TMA array. **(T)** Representative western blot image and quantification of CD47 total protein expression in FTs (n = 18) and SOCs (n = 19). **(U)** Pan-cancer analysis of CD47 exon 9 and 10 skipping level (PSI) in TCGA-OV comparing with normal tissue in GTEx database. **(V)** The relation of CD47 isoforms expression pattern with ferritin concentration based on the RNA FISH quantification result of Qilu cohort.

Supplementary Figure 2, related to Figure 2

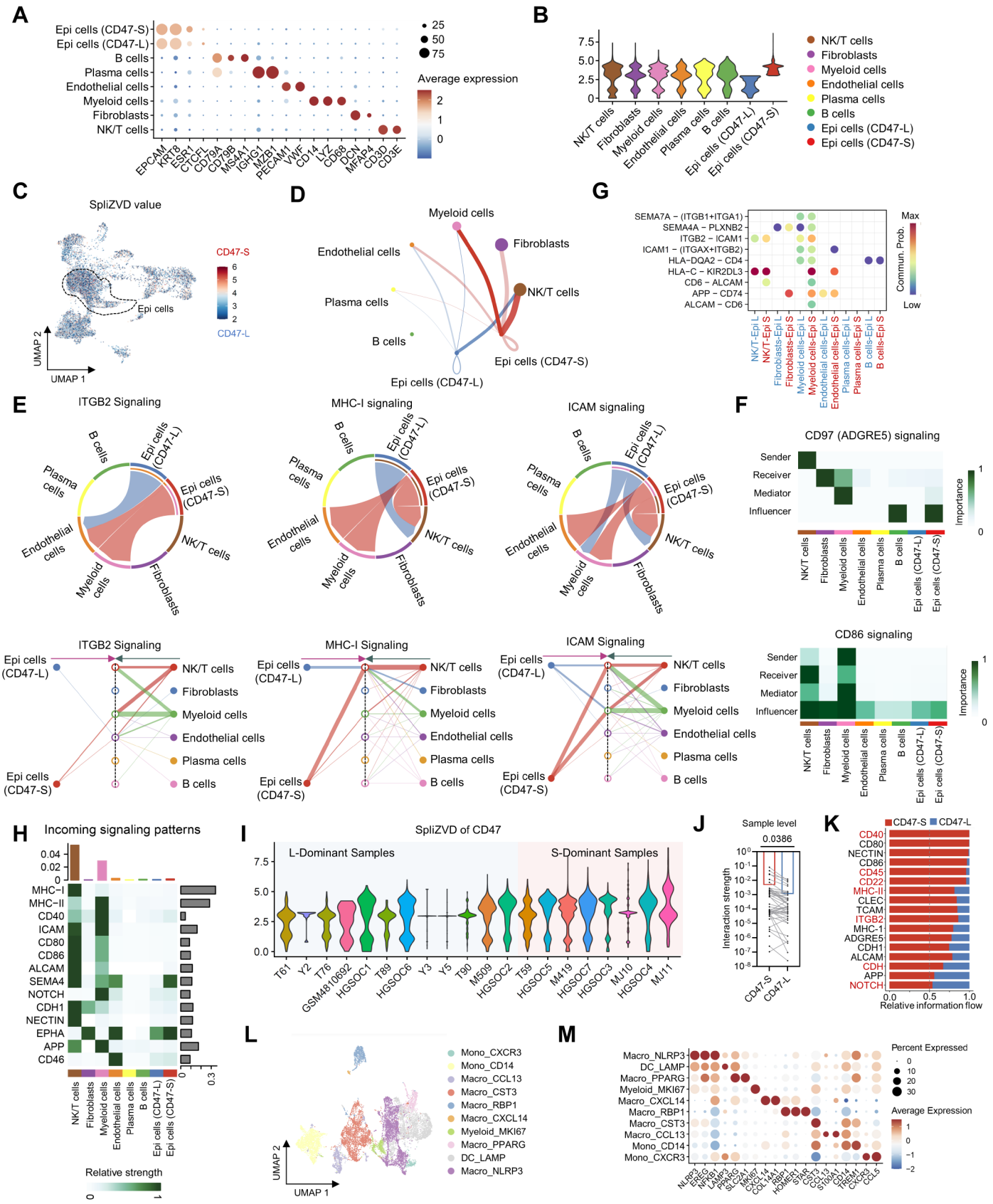

Supplementary Figure 2. Cell communication analysis of CD47-L and CD47-S epithelial cells or CD47-L/S dominant samples. (A) Normalized expression of marker genes in each cell cluster. **(B)** Violin plot of the SpliZVD value in CD47-L and CD47-S epithelial cells, myeloid cells, NK/T cells, B cells, pre-B cells and endothelial cells. **(C)** UMAP projection of SpliZVD value of all cells. Dashed circles indicate epithelial cell subgroup. Red, CD47-S cells; Blue, CD47-L cells. **(D)** Cell-cell communication network illustrating interactions between myeloid cells, fibroblasts, endothelial cells, NK/T cells, B cells, pre-B cells, CD47-L and CD47-S epithelial cells. The thickness of the connections represents the strength of the interactions. **(E)** Circos plot and network diagram indicated the interaction ratio of ITGB2, MHC-1, ICAM signaling among CD47-L and CD47-S epithelial cells, myeloid cells, NK/T cells, and endothelial cells. **(F)** CD97 (ADGRE5) and CD86 signaling heatmap depicting the roles of sender, receiver, mediator, and influencer cells. The color gradient reflects the interaction importance. **(G)** Dot plot showing the communication probability (Commun. Prob.) of ligand-receptor interactions between CD47-L/S epithelial cells and others. The color gradient represents communication strength, ranging from low (blue) to high (red), and dot size indicates interaction significance. **(H)** Heatmap of incoming signaling patterns showing relative signaling strength (color gradient) for various pathways across cell types. The bar plot on the right quantifies the overall relative signaling strength for each cell type. **(I)** SpliZVD value of CD47 in scRNA-seq data from 20 tissues. Average SpliZVD value over 3 was defined as S-dominant samples (red) while others were L-dominant samples (blue). **(J)** Quantification of the interaction strength of CD47-L/S dominant samples with other cell types. **(K)** Bar plot illustrating the relative information flow of ligand-receptor interactions mediated by CD47-S (red) and CD47-L (blue) isoforms. **(L)** UMAP projection of myeloid subgroups. **(M)** Dot blot of normalized expression of marker genes in each myeloid subgroup.

Supplementary Figure 3, related to Figure 2

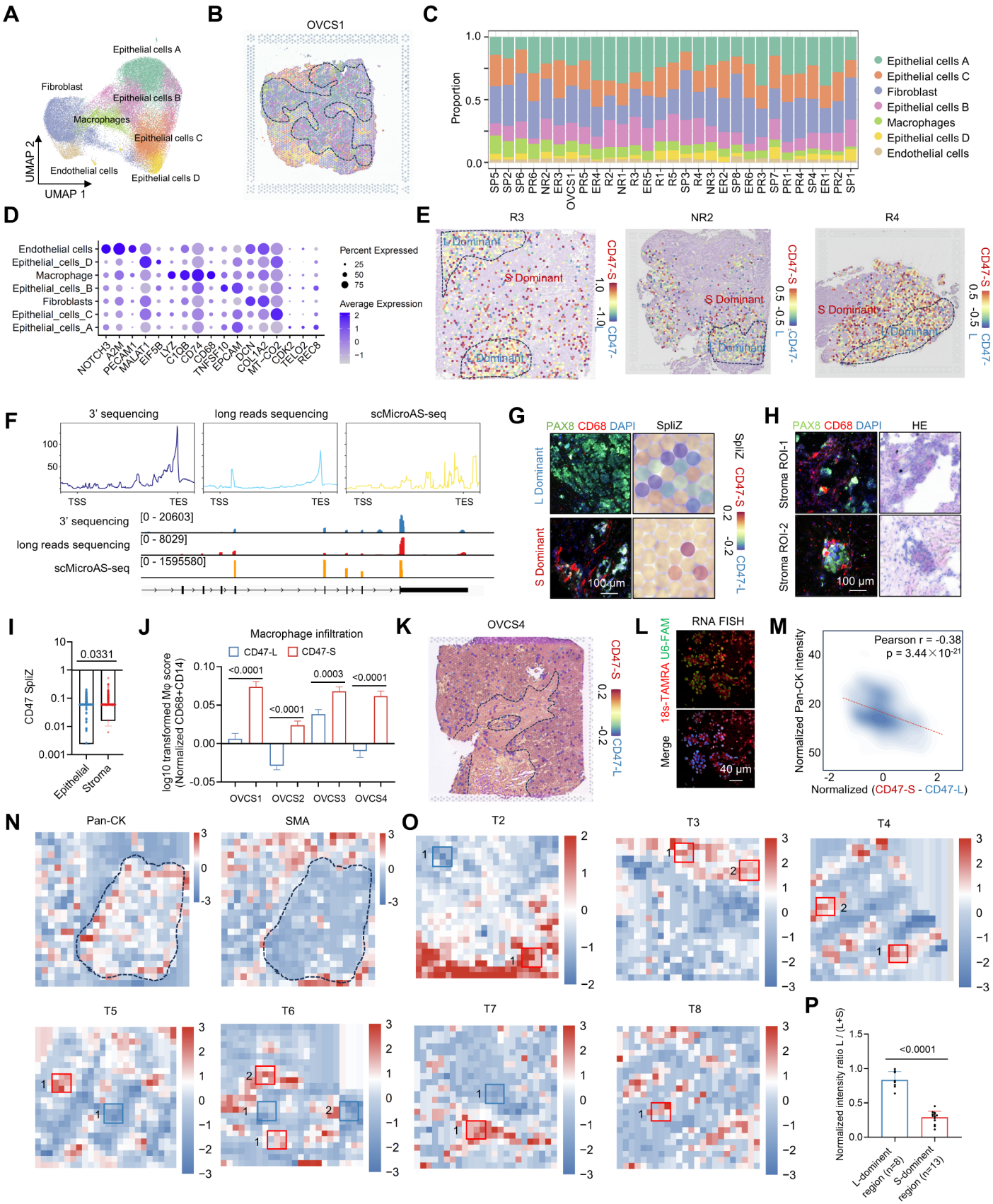

Supplementary Figure 3. Spatial distribution patterns of CD47-L/S isoforms. (A, B) UMAP projection of all spots **(A)** and spatial distribution map of OVCS1 tissue section **(B)**, colored by spot cluster. **(C)** Spots proportion of each cluster in 29 ovarian cancer tissues. **(D)** Normalized expression of marker genes in each spot cluster. **(E)** Spatial distribution map of CD47 SpliZ value cross the R3, NR2, and R4 tissue section. Dashed lines outline L-dominant epithelial cell region. **(F)** Genomic visualization of chromosome 3 genes (from TSS to TTS) and the CD47 locus using the 3' sequencing, long reads sequencing, and scMicroAS-seq data. **(G)** Immunofluorescence with adjacent sections of OVCS1 tissue. Green, PAX8; red, CD68; blue, DAPI. L-dominant (Blue) and S-dominant region (Red) were defined by SpliZ value correspond to the square in **Fig. 2P. (H)** Representative immunofluorescence image and adjacent HE stained image of two stroma regions in OVCS1 tissue. PAX8, green; CD68, red; DAPI, blue. **(I)** Quantification of CD47 SpliZ value in epithelial and stroma region. **(J)** The macrophage infiltration score (CD68 + CD14) of the spots from OVCS1, OVCS2, OVCS3, OVCS4 tissue sections. The data are presented as the mean ± SEM. Blue, CD47-L spots; red, CD47-S spots. **(K)** The spatial distribution map of CD47 SpliZ values calculated based on scMicroAS-seq data from the same spatial transcriptome cDNA library of the OVCS4 tissue. The color intensity of each spatial plot reflects SpliZ values. The dashed lines outline the epithelial cell region. **(L)** RNA FISH of 18s (red) and U6 (green) as a positive control. **(M)** Correlation analysis of normalized Pan-CK or SMA intensity and normalized (CD47-S - CD47-L). **(N)** Heatmap of Pan-CK and SMA intensity density (24×24 bins, middle). **(O)** Heatmap of normalized S-L value in T2, T3, T4, T5, T6, T7, T8, T9 tissues (24×24 bins). **(P)** Normalized intensity density ratio of CD47-L/(CD47-L+S) in L and S dominant regions from RNA FISH slides.

Supplementary Figure 4, related to Figure 3

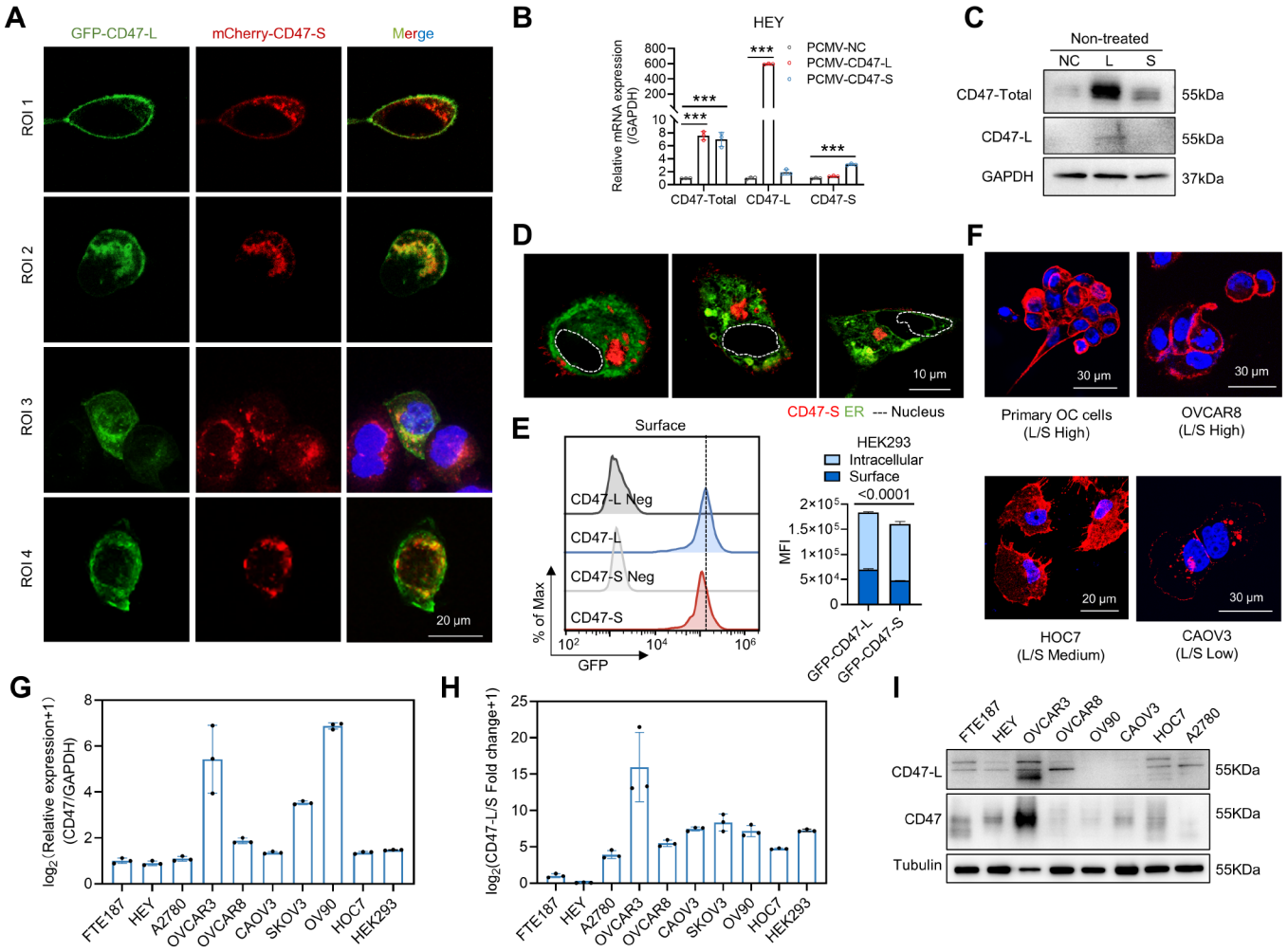

Supplementary Figure 4. Subcellular location and cell line expression of CD47-L/S isoforms. (A) Representative fluorescence images of four ROIs showing subcellular localization of GFP-CD47-L (green) and mCherry-CD47-S (red) in OVCAR3 cells. Scale bar, 20 μm. **(B, C)** mRNA and protein expression validation of CD47-L and CD47-S overexpression. Western blot used CD47 N-terminal antibody detecting total expression and C-terminal antibody detecting CD47-L. **(D)** Representative confocal microscopy images of OVCAR3 cells co-expressing CD47-S (pseudocolored red) and the ER marker DsRed2-ER (pseudocolored green). Scale bar, 10 μm. **(E)** Mean florescence intensity (MFI) of surface and intracellular CD47 expression in HEK293 cells detected by cell flowmetry. Unstained cells are shown in grey. Non-permeabilized cells show surface CD47 expression and permeabilized cells show total CD47 expression. The intracellular CD47 content was calculated as the difference between total CD47 and surface CD47 values. **(F)** Immunofluorescence assay detecting membrane and cytoplasmic CD47 expression in primary ovarian cancer cells (L/S high), OVCAR8 (L/S high), HOC7 (L/S medium), CAVO3 (L/S low) cells. **(G, H)** CD47 mRNA expression **(G)** and CD47-L isoforms ratio **(H)** in ovarian cancer cell lines, immortalized fallopian tube epithelial cell line FTE187 and HEK293. **(I)** Protein expression of CD47-L and CD47 total expression detected by western blot using antibodies targeting CD47 C-terminal and N-terminal.

Supplementary Figure 5, related to Figure 3

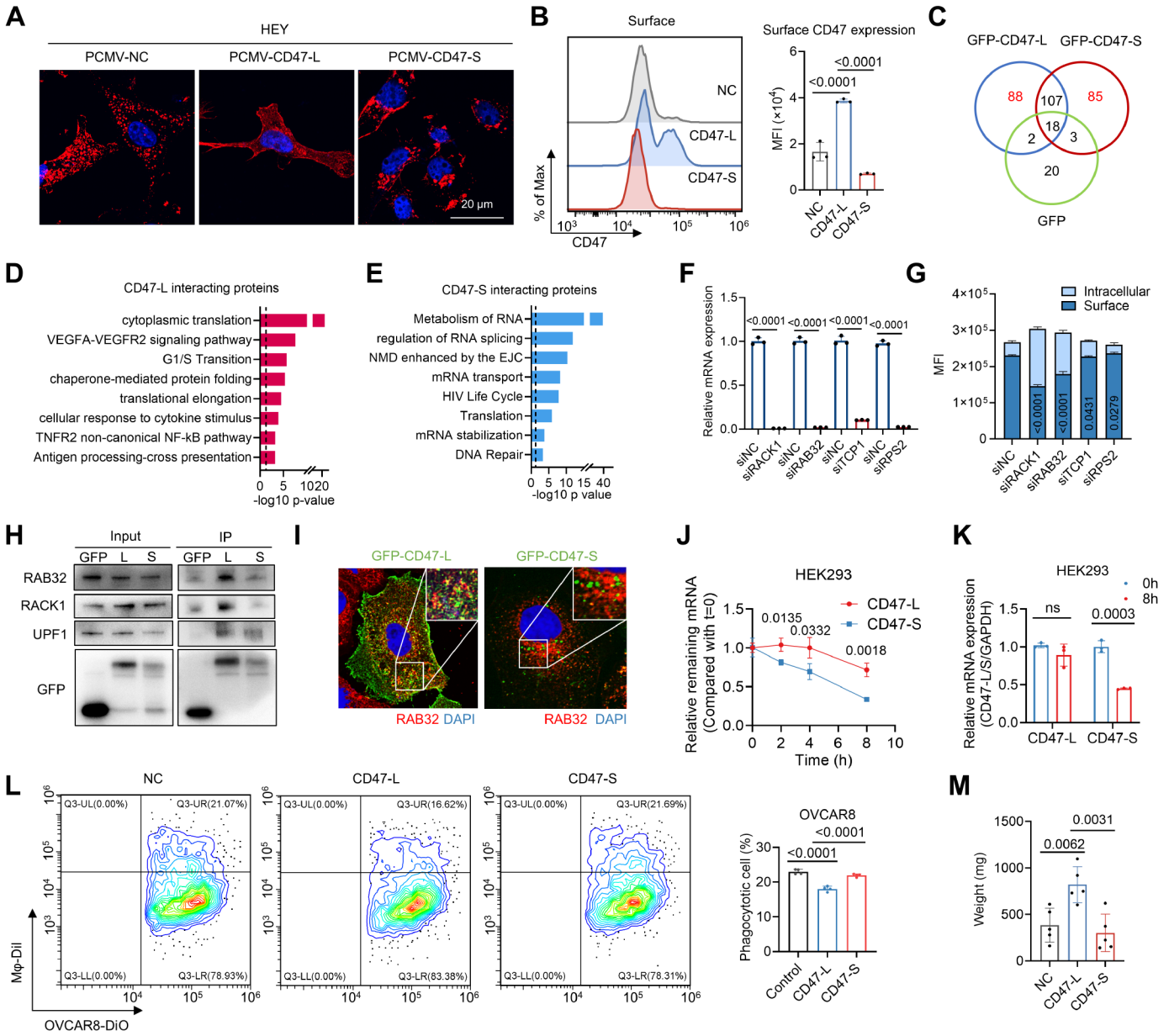

Supplementary Figure 5. RAB32-mediated vesicular transport promoted CD47-L distribution to plasma membrane. (A) Immunofluorescence assay detecting CD47 location in HEY cells after CD47-L and CD47-S overexpression. **(B)** MFI of surface CD47 in HEY cells overexpressing CD47-L and CD47-S as detected by flow cytometry. **(C)** Venn diagram of GFP-CD47-L and GFP-CD47-S interaction proteins detected by IP-MS. 88 proteins were GFP-CD47-L specific binding, while 85 proteins were GFP-CD47-S specific binding. **(D-E)** Pathway enrichment of GFP-CD47-L and -S specific binding proteins. **(F)** mRNA expression detected by qPCR after siNC, siRACK1, siRAB32, siTCP1, and siRPS2 transfection. **(G)** Cytoplasmic and membrane CD47 florescence intensity detected by cell flowmetry after silencing RACK1, RAB32, TCP1, and RPS2. **(H)** Western blot detected immunoprecipitated proteins with CD47-L/S isoform. RACK1 and RAB32 are interaction proteins specifically binding to the CD47-L isoform, while UPF1 is a common interacting partner for both isoforms. **(I)** Immunofluorescence assay detecting GFP-CD47-L/S and RAB32 location in HEY cells. **(J, K)** mRNA stability assay of CD47-L and CD47-S mRNA. The

remaining mRNA level was normalized to t=0. **(L)** Phagocytotic cell percentage of OVCAR8 cells overexpressing CD47-L and CD47-S. Dil and Dio double positive cell percentage of OVCAR8 overexpressing CD47-L and CD47-S co-cultured with macrophages. **(M)** Tumor weight of the xerograph mouse model after CD47-L/S overexpression.

Supplementary Figure 6, related to Figure 4

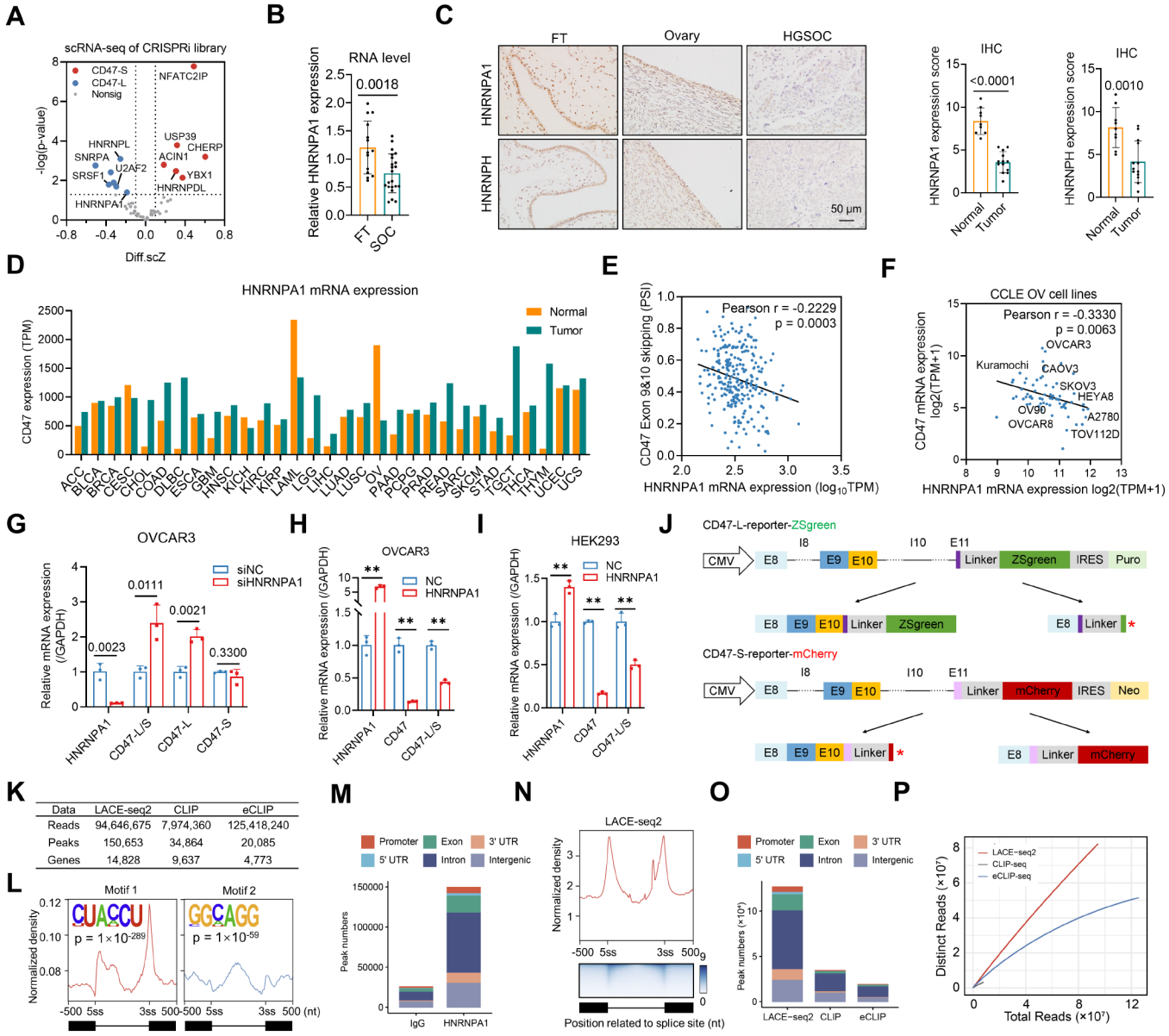

Supplementary Figure 6. HNRNPA1 regulates CD47-L/S isoform switch and its binding characteristics in ovarian cancer. (A) Volcano plot and of the positively (red) and negatively (blue) enriched core splicing factors after macrophage co-culturation. **(B)** qPCR detected HNRNPA1 mRNA expression in FTs and SOCs. **(C)** Immunohistochemical assay detected HNRNPA1 and HNRNPH protein expression in normal and SOC tissue. **(D)** Pan-cancer analysis of HNRNPA1 mRNA expression. **(E)** The correlation analysis between HNRNPA1 mRNA expression with CD47 exon skipping PSI. **(F)** Correlation analysis of the mRNA expression level of CD47 and HNRNPA1 in ovarian cancer cell lines in CCLE database. **(G)** mRNA expression levels of HNRNPA1 and CD47 isoforms after

knockdown HNRNPA1 in OVCAR3 cells. **(H-I)** mRNA expression levels of HNRNPA1, CD47 and its isoforms after overexpressing HNRNPA1 in OVCAR3 and HEK293 cells. **(J)** Schematic of the design of the CD47 multi-exon skipping reporter system based on the code-shifting strategy. The CD47-L-reporter-ZSgreen plasmid expresses ZSgreen after inclusion of exons 9 and 10, whereas the CD47-S-reporter-mCherry plasmid expresses mCherry after exon 9 and 10 skipping. **(K)** Read counts, peak numbers, binding genes of HNRNPA1 identified for HNRNPA1 by LACE-seq2, eCLIP-seq, and CLIP-seq. **(L)** HNRNPA1 binding motif 1 and 2 distributions related to the splice sites. **(M)** Binding peak numbers of IgG and HNRNPA1 groups identified by LACE-seq2. **(N)** Distribution of normalized binding signal of HNRNPA1 related to splice sites. **(O)** Genomic distribution of HNRNPA1 binding sites identified by LACE-seq2, eCLIP-seq, and CLIP-seq, showing peak counts across promoter, exon, 5'UTR, 3'UTR, intron, and intergenic regions. **(P)** Library viability was quantified by distinct reads number along with total reads.

Supplementary Figure 7, related to Figure 5

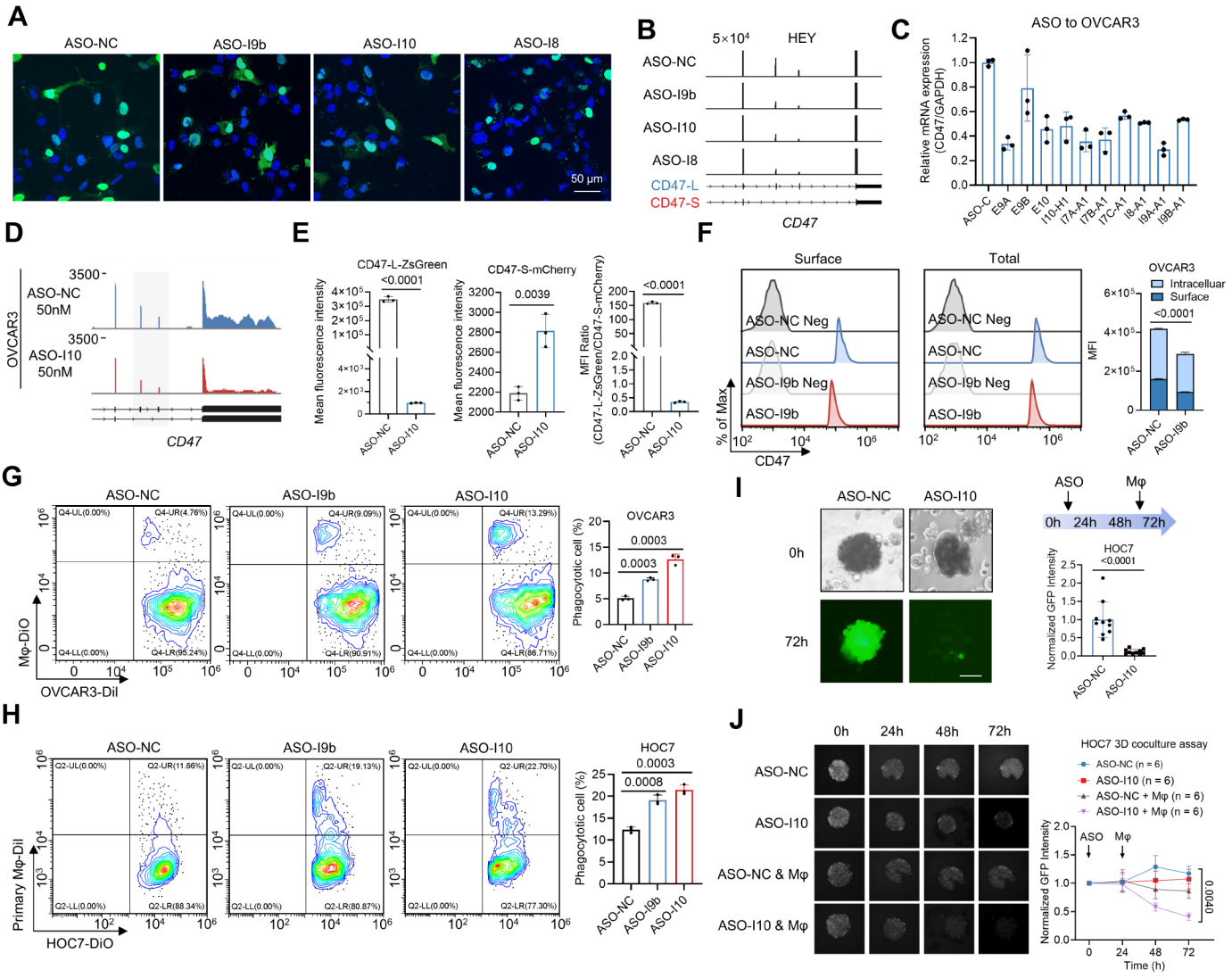

Supplementary Figure 7. ASOs targeting CD47 multi-exon skipping promote macrophage phagocytosis. (A) Confocal photographs of nucleoplasmic distribution after FAM labeled ASO transfection of HEY cells. **(B)** Genomic visualization of MicroAS-seq of OVCAR3 cells treated with ASO-NC, ASO-I8, ASO-I9b, ASO-I10. **(C)** Relative mRNA expression of CD47 after ASO screening. **(D)** Genomic visualization of total RNA-seq of OVCAR3 cells treated with 50 nM ASO-NC and ASO-I10. **(E)** Mean fluorescence intensity of CD47-L-ZsGreen and CD47-S-mCherry, and MFI ratio of OVCAR3-L/S-reporter cell line after ASO-I10 transfection. **(F)** Mean florescence intensity of surface and intracellular CD47 in OVCAR3 cells after ASO-I9b transfection. **(G-H)** Phagocytosis ratio after ASO-NC, ASO-I9b, and ASO-I10 transfection in OVCAR3 and HOC7 cells. OVCAR3 was cocultured with THP-derived macrophage and HOC7 was cocultured with BMDM-derived macrophage. **(I-J)** HOC7 cells 3D spheroids formed by HycopGel **(I)** or Nunclon Sphera 96 well plate **(J)** was co-cultured with macrophages and treated using ASO-I10. Normalized GFP fluorescence intensities were quantified.

Supplementary Figure 8, related to Figure 6

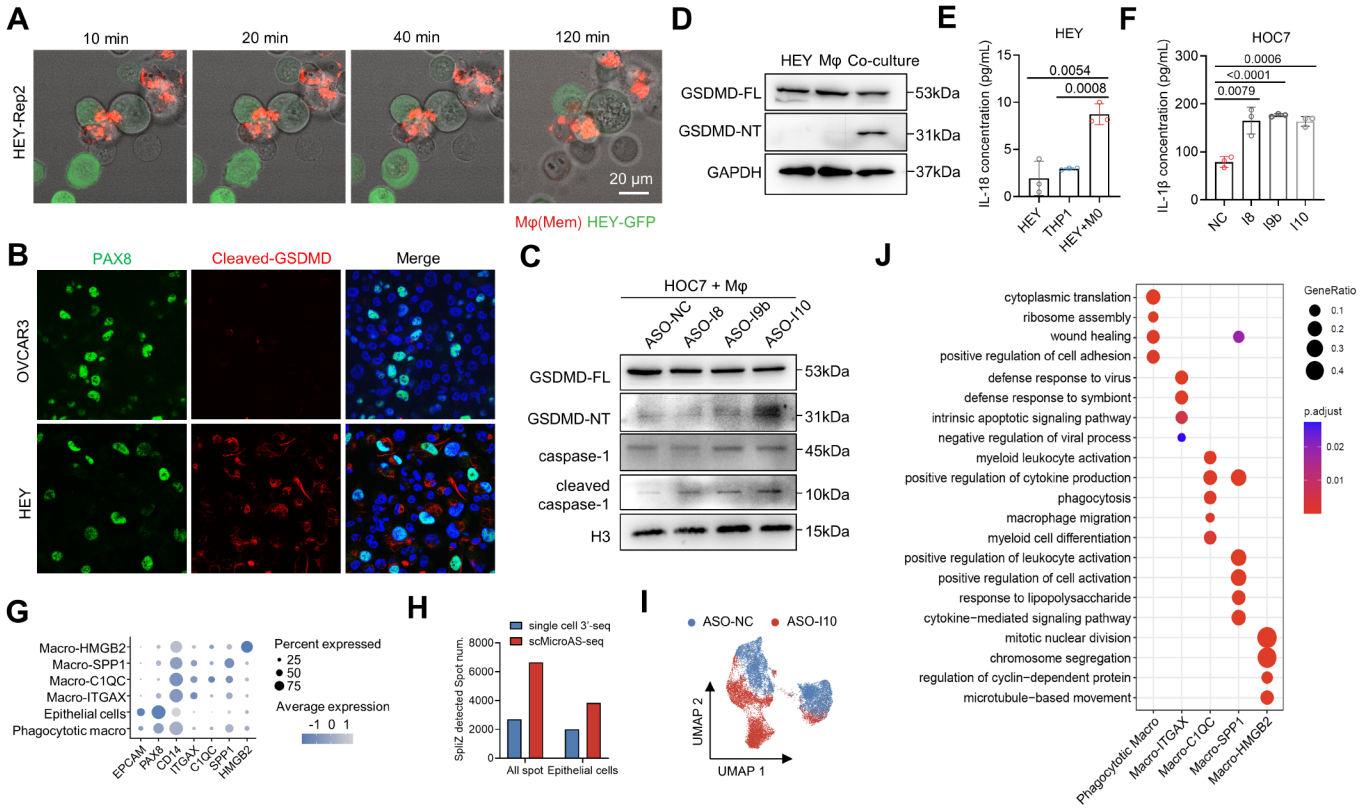

Supplementary Figure 8. ASO treatment induces macrophage-initiated pyroptosis of ovarian cancer cells. (A) Time-lapse photographs of HEY-GFP in co-culture with Dil-stained macrophages within 120 mins. **(B)** Distribution of PAX8 (Green) and Cleaved-GSDMD (Red) in untreated OVCAR3 and HEY cells co-cultured with macrophages was determined using immunofluorescence. **(C)** Protein expression of pyroptosis markers after ASO transfected HOC7 cells co-cultured with macrophages. **(D)** Protein expression of GSDMD-FL (full length) and GSDMD-NT (N-terminal) after HEY cancer cells co-cultured with macrophages. **(E)** IL-18 concentration in supernatants of HEY cells co-cultured with macrophages. **(F)** IL-1β concentration in supernatants of HOC7 cells co-cultured with macrophages. **(G)** Dot blot of normalized expression of marker genes in each cluster. **(H)** The number of SpliZ value detected spots in all spots and epithelial cells detected by single cell 3'-seq and scMicroAS-seq. **(I)** UMAP projection of scRNA-seq data from macrophages co-cultured with OVCAR3 cells transfected with ASO-NC or ASO-I10. **(J)** Pathway enrichment of marker genes of each macrophage subclusters.

Supplementary Figure 9, related to Figure 6

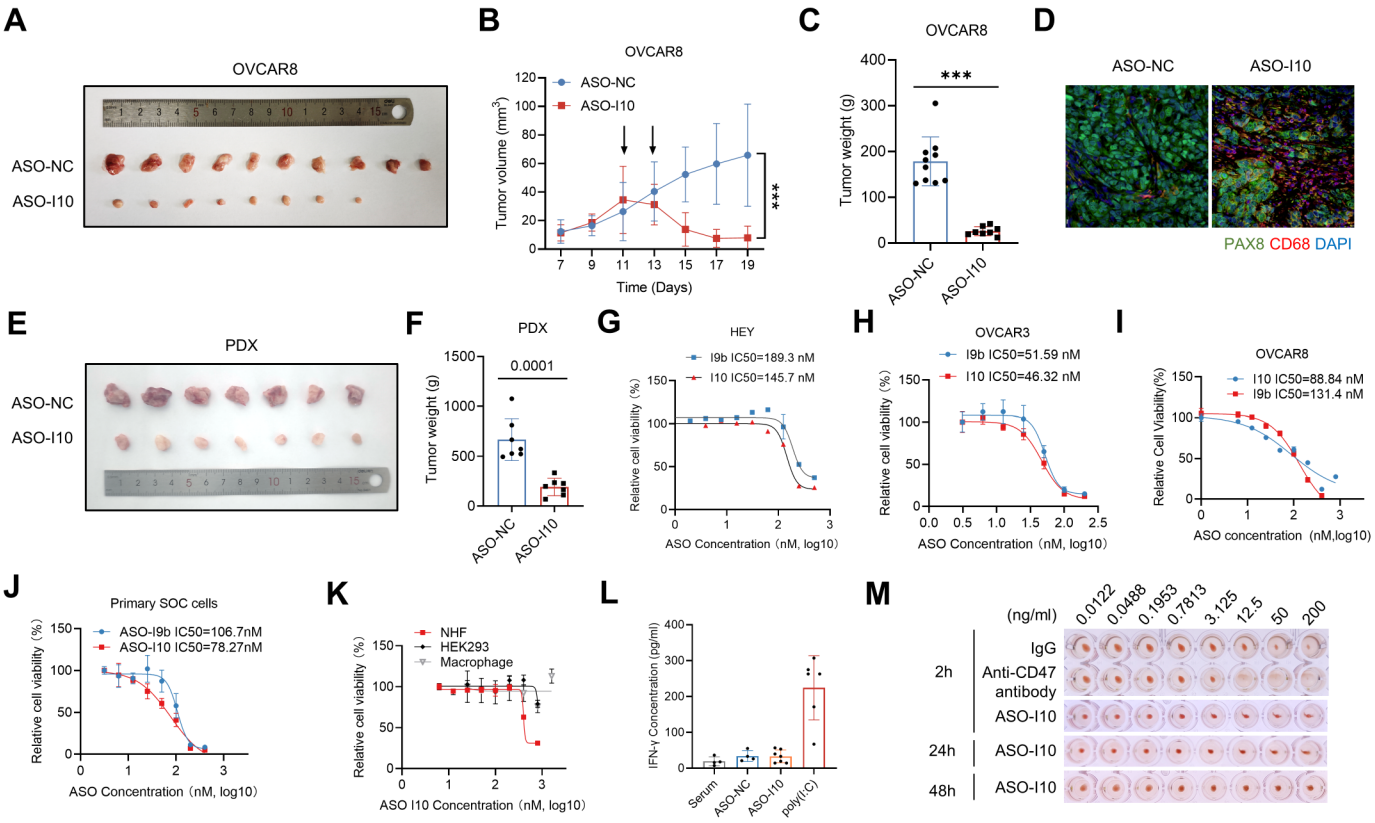

Supplementary Figure 9. ASO targeting CD47 isoform switch inhibits tumor growth in vivo and its immunogenicity and cytotoxicity. (A) Photographs of tumors after subcutaneous tumor formation in nude mice using the OVCAR8 cell line followed by administration of ASO intratumor injection. Two tumors in the ASO-I10 group were not palpable on Day 17. **(B)** Tumor volume over time in a nude mouse xenograft tumor model before and after administration of ASO-I10. A total of 2 intratumoral injections of ASO-I10 packaged in lipid nanoparticles were performed on days 11 and 13. **(C)** Tumor weight of the xenograft tumor model in ASO-NC (n = 10) and ASO-I10 (n = 8) group. **(D)** Immunofluorescence images of xenograft tumor model of ASO-NC and ASO-I10 groups. PAX8 (green) represents tumor cells and CD68 (red) represents macrophages. **(E)** Photographs of PDX tumors after subcutaneous tumor formation in immunodeficiency mice followed by administration of LNP packaged ASO intratumor injection (n = 7). **(F)** Tumor weight of the PDX tumor model in ASO-NC and ASO-I10 groups (n = 7). **(G-J)** Relative cell viability of HEY, OVCAR3, OVCAR8, and primary serous cancer cells after treatment of ASO-I9b and ASO-10 with gradient concentration. **(K)** Relative cell viability of immortalized normal human fibroblast NHF, HEK293, THP-1-derived macrophage after treatment of ASO-10 with gradient concentration. **(L)** Serum IFN-gamma level in mice after tail vein injection of ASO detected by ELISA. **(M)** RBC agglutination assay using RBC isolated from healthy donor and treated with ASO-I10 with gradient concentration and anti-CD47 Ab.